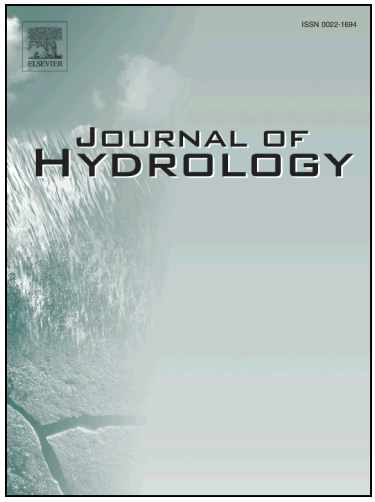

Research papers

The role of riparian vegetation density, channel orientation and water velocity in determining river temperature dynamics

Grace Garner, Iain A. Malcolm, Jonathan P. Sadler, David M. Hannah

PII: S0022-1694(17)30169-5
DOI: http://dx.doi.org/10.1016/j.jhydrol.2017.03.024
Reference: HYDROL 21881

To appear in: *Journal of Hydrology*

Received Date: 15 September 2015
Revised Date: 5 March 2017
Accepted Date: 13 March 2017

Please cite this article as: Garner, G., Malcolm, I.A., Sadler, J.P., Hannah, D.M., The role of riparian vegetation density, channel orientation and water velocity in determining river temperature dynamics, *Journal of Hydrology* (2017), doi: http://dx.doi.org/10.1016/j.jhydrol.2017.03.024

The role of riparian vegetation density, channel orientation and water velocity in determining river temperature dynamics

Grace Garner[a], Iain A. Malcolm[b], Jonathan P. Sadler[a] and David M. Hannah[a]

[a]School of Geography, Earth and Environmental Sciences, University of Birmingham, Edgbaston, Birmingham, B15 2TT, UK.

[b]Marine Scotland Science, Freshwater Laboratory, Faskally, Pitlochry, Perthshire, PH16 5LB, UK.

Email addresses: g.garner@bham.ac.uk; i.a.malcolm@marlab.ac.uk; j.p.sadler@bham.ac.uk; d.m.hannah@bham.ac.uk

Corresponding author: David Hannah, School of Geography, Earth and Environmental Sciences, University of Birmingham, Edgbaston, Birmingham, B15 2TT, UK. (d.m.hannah@bham.ac.uk)

ABSTRACT

A simulation experiment was used to understand the importance of riparian vegetation density, channel orientation and flow velocity for stream energy budgets and river temperature dynamics. Water temperature and meteorological observations were obtained in addition to hemispherical photographs along a ~1 km reach of the Girnock Burn, a tributary of the Aberdeenshire Dee, Scotland. Data from nine hemispherical images (representing different uniform canopy density scenarios) were used to parameterise a deterministic net radiation model and simulate radiative fluxes. For each vegetation scenario, the effects of eight channel orientations were investigated

by changing the position of north at 45° intervals in each hemispheric image. Simulated radiative fluxes and observed turbulent fluxes drove a high-resolution water temperature model for the reach. Simulations were performed under low and high water velocity scenarios. Both velocity scenarios yielded decreases in mean (≥ 1.6 °C) and maximum (≥ 3.0 °C) temperature as canopy density increased. Slow-flowing water resided longer within the reach, which enhanced heat accumulation and dissipation and drove higher maximum and lower minimum temperatures. Intermediate levels of shade produced highly variable energy flux and water temperature dynamics depending on the channel orientation and thus the time of day when the channel was shaded. We demonstrate that in many reaches relatively sparse but strategically located vegetation could produce substantial reductions in maximum temperature and suggest that these criteria are used to inform future river management.

1. INTRODUCTION

It is anticipated that a changing climate will alter river temperature regimes. Elevated temperatures relative to historical baselines are expected for most watercourses [e.g. *Beechie* et al., 2013; *van Vliet* et al., 2013; *MacDonald* et al., 2014a; *Hannah and Garner*, 2015]. Such changes, particularly increased maxima, may diminish the spatial and temporal extent of suitable cool-water habitat for temperature sensitive organisms with potential impacts on the composition and productivity of aquatic ecosystems [*Wilby* et al., 2010; *Leach* et al., 2012]. Consequently, there is substantial interest in adaptation strategies that may ameliorate the effects of climate warming, including: riparian planting [e.g. *Hannah* et al., 2008; *Brown* et al., 2010; *Imholt* et al., 2013; *Ryan* et al., 2013; *Garner* et al., 2014], reconnecting rivers to their floodplains [e.g. *Poole* et al., 2008; *Opperman* et al., 2010], restoring or enhancing hyporheic exchange [*Beechie* et al., 2013; *Kurylyk* et al., 2014], reducing and retaining urban runoff [e.g. *Booth and Leavitt*, 1999] and reducing rates of water abstraction [*Poole and Berman*, 2001]. However in upland streams, where catchment hydrology and geomorphology have not been altered significantly by human activities, fewer of these strategies may be implemented to protect aquatic ecosystems from thermal extremes [*Beschta*, 1997; *Poole and Berman*, 2001]. Observational datasets, frequently in combination with deterministic modelling approaches, have demonstrated that the summer temperature of headwater streams is generally dominated by: (1) advected heat from upstream (2) heat exchange at the air-water column interface [e.g. *Westhoff* et al., 2011; *Leach and Moore*, 2014; *MacDonald* et al., 2014a; *Garne*r et al., 2014], predominantly solar radiation gains [*Hannah* et al., 2008; *Leach and Moore*, 2010; *MacDonal*d et al., 2014a], and at some locations (3)

groundwater inflows [e.g. *Westhoff* et al., 2007]. Recognising the important role of energy exchange between the atmosphere and the water column and in response to the increasing scientific literature, river managers (e.g. The River Dee Trust; Upper Dee riparian scheme) are increasingly advocating the use of riparian vegetation to reduce total energy inputs to the water column, and thus thermal variability and extremes [e.g. *Gomi* et al., 2006; *Johnson and Jones*, 2000; *Hannah* et al., 2008; *Imholt* et al. 2011, 2013; *Garner* et al., 2015].

Although there is a clear requirement for understanding of the effects of riparian cover on stream temperature, there have been relatively few robust process based studies that provide realistic predictions of the likely effects of landuse change. *Moore* et al. [2014] discussed various methods for representing the effects of vegetation on radiative energy fluxes above streams. However, to date river temperature models [e.g. *Rutherford* et al., 1997; *Watanabe* et al., 2005; *DeWalle*, 2008; *Roth* et al., 2010; *Lee* et al., 2012] have not considered the importance of vegetation structure (i.e. leaves, trunks and branches) and location relative to the position of the sun and the receiving waterbodies. Therefore, they were unable to adequately account for the temporally variable influence of discontinuous vegetation on the radiation budget. Furthermore, vegetation also has a significant effect on riparian microclimatic variables such as wind speed, relative humidity and air temperature, resulting in large reductions in latent heat losses (e.g. 60-87 % was observed by *Garner* et al., 2015) in comparison to open reaches [e.g. *Hannah* et al., 2008; *Garner* et al., 2015]. However, most modelling studies [e.g. *Rutherford* et al., 1997; *Watanabe* et al., 2005; *DeWalle*, 2008; *Lee* et al., 2012] have not considered the effects of changing microclimate as a result of riparian landuse change and so likely

over-estimated the effect of forest canopies on reducing net energy fluxes and thus water temperature. Consequently, attempts to simulate the effects of riparian landuse change on water temperature have lacked the necessary physical realism to produce accurate estimates of effect sizes.

This study aims to generate systematic, process-based information on the effects of: (1) channel shading, (2) channel orientation and (3) water velocity on river temperature. Previous modelling and observational studies suggest that these three variables play an important role in determining river temperature dynamics. Firstly, because water temperatures are lower when vegetation is present [e.g. *Hannah* et al., 2008; *Hrachowitz* et al., 2010; *Roth* et al., 2010; *Garner* et al., 2015] and instantaneous differences in temperature between forested and open locations are greatest at sites under the densest canopies [e.g. *Roth* et al., 2010; *Broadmeadow* et al., 2011; *Groom* et al., 2011; *Imholt* et al., 2013]. Secondly, because the orientation of the channel [*LeBlanc*, 1997; *DeWalle*, 2008; *Li* et al., 2012] and therefore the location of vegetation relative to the path of the sun is important in controlling solar radiation inputs [*Lee* et al., 2012]. Finally, because longitudinal temperature gradients are reduced in steeper, faster flowing reaches compared with flatter, slower flowing ones [e.g. *Danehy* et al., 2005; *Subeh*i et al., 2009; *Groom* et al., 2011]. Knowledge of these controls and their interactions is important to inform optimal tree planting strategies and to assess likely outcomes.

In this context, we simulate the effects of varying riparian vegetation density and channel orientation on the stream energy budget and quantify their influence on water temperature dynamics under scenarios of high and low water velocity. The effects of

riparian vegetation on river temperature are modelled using hemispheric photographs of different riparian canopy densities under field observed conditions and local measurements of micro-climate, thereby providing improved realism to estimates of likely effect size while at the same time being sufficiently generalisable to provide useful information to inform riparian planting strategies.

2. STUDY AREA

We collected field data within a 1050 m study reach of Glen Girnock. This upland basin is located in north east Scotland and drains into the Aberdeenshire Dee (Figure 1). The catchment upstream of the reach has an area of ~ 22 km^2 in which heather (*Calluna*) moorland dominated landuse. Riparian landuse along the reach transitioned from moorland to semi-natural forest composed of birch (*Betula*), Scots pine (*Pinus*), alder (*Alnus*) and willow (*Salix*) [*Imholt* et al., 2010]. Basin soils are composed predominantly of peaty podsols with some peaty gleys. Basin geology is dominated by granite at higher elevations and schists at lower elevations and is thus relatively impermeable [*Tetzlaff* et al., 2007]. Within the study reach the riverbed is composed primarily of cobble and boulder with gravel accumulation in localised patches. The reach is 280 m above sea level (asl) at the upstream reach boundary and 255 m asl at the downstream reach boundary. During field data collection the mean wetted width of the channel was 9.5 m. Previous work within the study reach demonstrated that there are no substantial groundwater inflows and consequently that groundwater does not significantly modify water temperature dynamics [*Malcolm* et al., 2005; *Garner* et al., 2014]. Thus, the influence of canopy density, channel orientation and water velocity on water temperature could be investigated in the absence of confounding groundwater influences [e.g. *Story* et al., 2003; *Westhoff* et al., 2011].

The UK Meteorological Office record daily averages of air temperature and totals of precipitation at Balmoral (< 10 km north west of the catchment). During the period 1950-2013 annual average air temperature was 6.6 ℃, maximum temperatures occurred in June and July (daily averages 13.0 and 12.6 ℃ respectively) and minima occurred December to February (daily averages 2.4, 2.2 and 1.6 ℃ respectively). Between 1950 and 2013 annual average precipitation totalled 846 mm, October to January were the wettest months (daily average totals ranged from 85.7 mm in December to 92.5 mm in October) and February to September were the driest (daily average totals ranged from 55.1 mm in April to 70.8 mm in August). River discharge is monitored continuously by the Scottish Environmental Protection Agency (SEPA) in a rated natural section of the Girnock at Littlemill (Figure 1). Annual mean flow is 0.530 m^3s^{-1} (1969- 2013). Summer flows (i.e. June-August) are typically < 0.100 m^3s^{-1} but the flow regime is highly responsive to precipitation and so high flow events (e.g. ≥ Q_{10}, 1.126 m^3s^{-1}) occur year-round.

3. METHODS

3.1. Experimental design

Spatially distributed field data were used to parameterise a simulation experiment that investigated the influence of: (1) riparian vegetation density, (2) channel orientation (and thus vegetation orientation relative to the sun's path), and (3) water velocity (a proxy for stream gradient) on heat exchange patterns and water temperature dynamics within a 1050 m reach of the Girnock Burn. A single time series of discharge was used for each velocity scenario thereby separating the the effects of velocity and

residence time from those of varying water volume. Consequently, the effects of each vegetation and channel orientation scenario were simulated for a low (i.e. slow velocity: 0.023 ms^{-1}) or high gradient (i.e. fast velocity: 0.155 ms^{-1}) river. We did not investigate the effects of changing discharge because we were primarily interested in the effects of riparian woodland on river temperature under summer low flow conditions, when the most extreme high water temperatures are expected to occur.

Firstly, a process-based water temperature model (herein referred to as the 'base model') driven by spatially distributed energy flux data temperature [*Garner* et al., 2014 after *Bartholow*, 2000; *Boyd and Kasper*, 2003; *Rutherford* et al., 2004; *Westhoff* et al., 2007, 2010; *Leach and Moore*, 2011; *MacDonald* et al., 2014a, b] was parameterised for observed conditions within the Girnock Burn. Previous work suggested that the base model adequately described spatio-temporal variability in river temperature [*Garner* et al., 2014], and thus is capable of providing realistic assessments of the effects of interest. Secondly, simulations representative of varying vegetation density, channel orientation and water velocity scenarios were performed by adjusting selected parameters (see sections '3.2 Data' and '3.3 Estimation of stream energy budget components') in the base model (herein referred to as the 'simulation experiments').

For the simulation experiments, nine hemispherical images obtained in the field (Figure 2; termed 'vegetation scenarios' herein) were used to represent different canopy densities (i.e. 10- 90 % in 10 % increments). The images were used to parameterise a deterministic net radiation model [*Leach and Moore*, 2010] and simulate radiative fluxes at 1 m intervals indicative of uniform forestation of the

entire reach. The effect of channel orientation on energy exchanges and water temperature was investigated for each vegetation scenario by changing the location of north and thus the path of the sun relative to the position of vegetation in each hemispherical image at 45-degree intervals (see sun-paths on Figure 2). Thereby, we simulated the effects of each vegetation scenario on north-south (N-S), northeast-southwest (NE-SW), east-west (E-W), southeast-northwest (SE-NW), south-north (S-N), southwest-northeast (SW-NE), west-east (W-E) and northwest-southeast (NW-SE) flowing streams. Modelled radiative fluxes were combined with linearly interpolated turbulent fluxes (i.e. sensible and latent heat) calculated from measured micro-meteorological variables at the three automatic weather stations (Fig. 1, see below for further details) to drive the water temperature model for each scenario. Stream temperature was predicted along the reach at a resolution of 50 m.

3.2. Data

Field data were collected between October 2011 and July 2013 [from *Garner* et al., 2014]; hydrometeorological data collected on 6 July 2013 (Figure 3) were chosen to meet the aim of the present study. On this day, measured water temperatures (Figure 3a) and solar radiation gains to the water column (Figure 3b) at an automatic weather station (AWS) sited within the reach on open moorland ($AWS_{open;}$ Figure 1) were high, while discharge was very low. Consequently, the effects of vegetation density, channel orientation and water velocity on water temperature were evaluated under a 'worst-case scenario' of high energy inputs and low flows [after *Garner* et al., 2014].

3.2.1. Micrometeorological measurements

Three AWSs (automatic weather stations) were installed within the reach (Figure 1) to characterise spatio-temporal variability in energy fluxes: the first was located in open moorland at the upstream reach boundary (AWS_{open}), the second was located in semi-natural forest 190 m downstream of the upstream boundary (named "AWS forest upstream" or AWS_{FUS}) and the third was located in semi-natural forest 685 m downstream of the upstream boundary (named "AWS forest downstream" or AWS $_{FDS}$). Hydrometeorological variables measured by each AWS were: air temperature (°C), relative humidity (%), wind speed (ms^{-1}), incoming solar radiation, net radiation and bed heat flux (all Wm^{-2}). The instruments deployed on the AWSs are detailed in *Hannah* et al. [2008]. AWSs measured meteorological variables ~2 m above the stream surface. Bed heat flux measurements were made using heat flux plates buried (to avoid radiative and convective errors) at 0.05 m depth within the riverbed below each AWS. Heat flux plates provided aggregated measurements of convective, conductive, advective and radiative heat exchanges between the atmosphere and the riverbed and the riverbed and the water column [after *Evans* et al., 1998; *Hannah* et al., 2008; *Garner* et al., 2014]. All AWS sensors were sampled at 10-second intervals and averages were logged every 15-minutes.

3.2.2. Stream temperature measurements

Stream temperature measurements were used to evaluate the performance of the base model under observed conditions [i.e. *Garner* et al., 2014] and provided initial conditions at the upstream reach boundary. Water temperature was measured at 15-minute intervals using ten water temperature TinyTag Aquatic 2 dataloggers (manufacturer stated accuracy of +/- 0.5 °C) and three Campbell 107 thermistors (manufacturer stated accuracy +/- 0.1 °C) connected to AWSs (automatic weather

stations) and installed at 0 (AWS_{Open}), 190, 315, 460, 565, 630, 685 (AWS_{FUS}), 760, 815, 865, 940 1015 and 1050 (AWS_{FDS}) m downstream of the upstream reach boundary (Figure 1). Prior to installation the sensors were compared [following Hannah et al., 2009] over the range 0-30 °C and were in agreement by < +/- 0.1 °C. Sensors were deployed within white plastic PVC tubes to shield them from direct solar radiation.

3.2.3. Hydrology and stream geometry

Discharge (m^3s^{-1}) was obtained from a Scottish Environmental Protection Agency (SEPA) gauging station at Littlemill (Figure 1). Discharge was required as input to the water temperature model (see "3.4 Modelling approach"). The time series of discharge from 6th July 2013 (Figure 3e) was used as input to the base model run and for the simulation experiment runs; values were very low (average 0.089 m^3s^{-1}, which is equal to Q_{96} calculated for June- August during the period 1983-2013), stable (0.082- 0.096 m^3s^{-1}) and exhibited no sudden changes. Water velocity (ms^{-1}) for the base model was calculated from discharge using a discharge- mean velocity function for Littlemill derived by *Tetzlaff* et al. [2005] and was used to route discrete parcels of water through the reach in order to drive the flow-routing component of the water temperature model (see '*3.4 Modelling approach'*). For evaluation of the base model velocity was allowed to vary temporally (at hourly intervals) in response to changing discharge. For the simulation experiments constant values of high (0.155 ms^{-1}) and low velocity (0.023 ms^{-1}) were used at all locations and time steps. Wetted width was required as input to the water temperature model. Spatially varying values measured at 50 m intervals along the reach were used for the base model evaluation, but a fixed value of 9.5 m (the mean wetted width) was used for the simulation experiments.

3.2.5. Hemispherical images

Hemispherical images were taken at 5 m intervals along the stream centreline using a Canon EOS-10D 6.3 megapixel digital camera with Sigma 8 mm fisheye lens. Prior to taking each image the camera was orientated to north and levelled ~20 cm above the stream surface [after *Leach and Moore*, 2010]. All images were used to parameterise the radiation component of the base model and thus represent the baseline (current) riparian vegetation condition in the reach [i.e. *Garner* et al., 2014] for the model validation. Data derived from nine of these images (each representative of 10-90 % canopy density at 10 % increments; Figure 2) were used to parameterise the vegetation scenarios.

3.3. Estimation of stream energy budget components

3.3.1. Net energy

Net energy (Qn, Wm^{-2}) available to heat or cool the water column was calculated as:

$$Q_n = Q^* + Q_e + Q_h + Q_{bhf} \quad \text{(Equation 1)}$$

Where Q_n is net energy, Q^* is net radiation, Q_e is latent heat, Q_h is sensible heat and Q_{bhf} is bed heat flux (all Wm^{-2}). Heat from fluid friction was omitted because it makes a negligible contribution to the energy budget in this reach [after *Garner* et al., 2015]. Herein, positive energy fluxes represent gains to the water column while negative energy fluxes represent losses.

3.3.2. Net radiation

A deterministic model developed by *Moore* et al. [2005] and then extended and evaluated by *Leach and Moore* [2010] was used to compute net radiation (Q^*) at the location of each hemispherical image. At each location net radiation was calculated as:

$$Q^* = K^* + L^* \quad \text{(Equation 2)}$$

Where K^* (Wm^{-2}) is net shortwave radiation (Equation 3) and L^* (Wm^{-2}) is net longwave radiation (Equation 4).

$$K^* = (1 - \alpha)[D(t)g(t) + s(t)f_v] \quad \text{(Equation 3)}$$

$$L^* = [f_v\varepsilon_a + (1 - f_v)\varepsilon_{vt}]\sigma(T_a + 273.2)^4 - \varepsilon_w\sigma(T_w + 273.2)^4 \quad \text{(Equation 4)}$$

Where α is the stream albedo, $D(t)$ is the direct component of incident solar radiation at time t (Wm^{-2}), $g(t)$ is the canopy gap fraction at the position of the sun in the sky at time t, $s(t)$ is the diffuse component of solar radiation (Wm^{-2}), f_v is the sky view factor, ε_a, ε_{vt} and ε_w are the emissivity of the temperatures of the air, vegetation and water respectively (all °C), σ is the Stefan-Boltzmann constant (5.67×10^{-8} Wm^{-2} K^{-4}), and T_a and T_w are air and water temperature respectively (both °C).

Values for atmospheric emissivity were calculated for clear-sky day and night conditions using the equation presented in *Prata* [1996; used also by *Leach and Moore*, 2010, *Garner* et al., 2014] and were subsequently adjusted for cloud cover using equations in *Leach and Moore* [2010]. The emissivity and albedo were taken to

be 0.95 and 0.05 for water, and 0.97 and 0.03 for vegetation respectively [after *Moore* et al., 2005 and used subsequently by *Garner* et al., 2014].

Gap fractions (g_*) were computed as a function of solar zenith angle (θ,°) and solar azimuth (ψ,°), $g_*(\theta, \psi)$, which were derived at 5 ° intervals from analysis of the hemispherical photographs with Gap Light Analyser software [*Frazer* et al., 1999]. Hemispherical photographs were converted to binary images by setting a threshold that determines whether a pixel should be classified as sky (white) or another object (black) such as river banks, tree trunks, leaves or branches. An optimum threshold value of 130 was selected from candidate values of 120-190 at 10 unit increments. This threshold value minimised RMSE between observed and modelled incoming solar radiation at AWS_{FUS} during 1 and 7 July 2013 [see Garner et al., 2014]. The solar zenith and azimuth angles were computed as a function of time (*t*, minutes) using equations in *Iqbal* [1983] so that the canopy gap at the location of the sun could be derived from $g^*(\theta,\psi)$ as a function of time, $g(t)$. Sky view factor was computed as:

$$f_v = \frac{1}{\pi}\int_0^{2\pi}\int_0^{\pi/2} g_*(\theta,\psi)\cos\theta\sin\theta * d\theta * d\psi$$

(Equation 5)

Solar radiation measured at AWS_{open} was used to drive the solar radiation model for evaluation of the base model and the simulation experiments in order to simulate this energy flux at 1 m intervals along the reach centreline. For the simulation experiments, time series of air temperature (used to calculate net longwave radiation) were generated by linear interpolation between the two nearest AWSs to the point along the stream centreline at which the hemispherical photograph representative of

the vegetation scenario was taken. Net longwave radiation is a function of water temperature; therefore initial values for this flux at the upstream reach boundary were calculated using observed water temperature at AWS_{Open}.

3.3.3. Latent and sensible heat fluxes

To compute heat lost by evaporation or gained by condensation, latent heat was estimated after *Webb and Zhang* [1997] (Equation 6).

$$Q_e = 285.9(0.132 + 0.143 * U)(e_a - e_w)$$

(Equation 6)

Where U is wind speed (ms^{-1}) and e_a and e_w are vapour pressures of air and water (both kPa), respectively. Saturation vapour pressure (e_{sat}) was calculated as a function of air or water temperature, T (K), after Stull [2000] (Equation 7).

$$e_{sat}(T) = 0.611 * exp\left[\frac{2.5*10^6}{461} * \left(\frac{1}{273.2} - \frac{1}{T}\right)\right]$$

(Equation 7)

Vapour pressure of water (e_w) was assumed to be equal to $e_{sat}(T_w)$. Vapour pressure of air (e_a) was calculated using Equation 8.

$$e_a = \frac{RH}{100} e_{sat}(T_a)$$ (Equation 8)

Sensible heat (Equation 9) was calculated as a function of Q_e (Equation 6) and Bowen ratio (β) (Equation 10), where P is air pressure (kPa).

$Q_h = Q_e * \beta$ (Equation 9)

$\beta = 0.66 * \left(\frac{P}{1000}\right) * [(T_w - T_a)/(e_a - e_w)]$ (Equation 10)

For the simulation experiments, time series of meteorological variables (i.e. air temperature, wind speed and relative humidity) required to calculate turbulent fluxes were generated for each vegetation scenario by linear interpolation between the two nearest AWSs to the point along the stream centerline at which the hemispherical photograph representative of the scenario was taken. Turbulent fluxes are a function of water temperature; therefore initial values at the upstream boundary were calculated using observed water temperature at AWS_{Open}.

3.4. Modelling approach

A Lagrangian modelling approach was used to simulate river water temperature [after *Garner* et al., 2014] in which the trajectory of discrete parcels of water is followed through the reach in order to determine the energy exchange conditions the parcels are exposed to and thus calculate changes in their temperature as they flow downstream and time elapses.

The reach was divided into a series of 1 m segments (s) bounded by nodes (x). At hourly intervals a discrete parcel of water (i) with an initial temperature was released from the upstream boundary at AWS_{Open} and routed through the reach using the discharge-mean velocity function [Tetzlaff, 2005]. The distance travelled by each water parcel from its location (x) at time t to its next location ($x+1$) at time $t+\Delta t$ was

calculated as the product of the length of each 15-minute time step (Δt, i.e. 900 seconds) and either: (1) for evaluation of the base model, the average velocity of the parcel at times t and $t+\Delta t$ or (2) for the simulation experiments, 0.023 or 0.155 ms^{-1} for the low and high velocity scenarios, respectively. As the water parcel travelled downstream from x towards $x+1$ the model determined the mean of each of the meteorological variables the parcel was exposed to along its trajectory through the segments at times t and $t+1$. This information was used to calculate the water temperature of each parcel at 50 m intervals by integration of Equation 11 in the deSolve package [*Soetaert* et al., 2010] for R (Version 3.0.2, R Group for Statistical Computing, 2013).

$$\frac{\partial T_{w\,(i)}}{\partial x} = \frac{\left[\left[w_{\bar{s}}(Q_{n\,(\bar{s},t)}) + w_{\bar{s}}(Q_{n(\bar{s},t+\Delta t)})\right]/2\right]}{C\left[\left(F_{(\bar{s},t)} + F_{(\bar{s},t+\Delta t)}\right)/2\right]} \quad \text{(Equation 11)}$$

Where $w_{\bar{s}}$ is the mean wetted width of the stream surface (m) within segments $\bar{s}$, $K^*_{\overline{(\bar{s},\mathrm{t}/\,\mathrm{t}+\Delta t)}}$, $L^*_{\overline{(\bar{s},\mathrm{t}/\,\mathrm{t}+\Delta t)}}$, $Q_{e\,\overline{(\bar{s},\mathrm{t}/\,\mathrm{t}+\Delta t)}}$, $Q_{h\,\overline{(\bar{s},\mathrm{t}/\,\mathrm{t}+\Delta t)}}$ and $Q_{bhf\,\overline{(\bar{s},\mathrm{t}/\,\mathrm{t}+\Delta t)}}$ are the mean net shortwave, net longwave, latent, sensible and bed heat fluxes within segments $\bar{s}$ at time t or $t+\Delta t$. C is the volumetric heat capacity of water (4.18 x 10^6 Jm^{-3} $°C^{-1}$) and $F_{\overline{(\bar{s},\mathrm{t}/\,\mathrm{t}+\Delta t)}}$ is the discharge [m^3s^{-1}] within segments $\bar{s}$ at time t or $t+\Delta t$. In 'Supplement 1' we discuss the principles of Equation 11.

Energy exchange due to bed heat flux, which accounted for < 1 % of the stream energy budget [*Garner* et al., 2014], was retained within the model structure for evaluation of the performance of the base model but omitted for the simulation experiments so as to investigate the influence of vegetation scenarios on water

temperature dynamics driven by energy exchanges between the atmosphere and the water column only.

4. RESULTS

4.1. Stream energy budget

4.1.1. Net solar radiation

For each vegetation scenario and channel orientation, simulated daily total net solar radiation flux is demonstrated in Figure 4a while the underlying diurnal patterns are demonstrated in Figure 5. Total net energy flux typically decreased as vegetation density increased (Figure 4a). The orientation of the channel had a limited impact on total daily net solar radiation gains under: (1) the densest canopies (i.e. 70- 90 % density; Figure 4a), when limited portions of the stream remained unshaded (Figure 2c- 2f) and (2) under the sparsest canopies (i.e. ≤ 20 %; Figure 4a), when vegetation did not overhang the stream, cast minimal shade regardless of channel orientation (Figure 2a and 2b) and diurnal patterns were similar regardless of channel orientation (scenarios of 10 and 20 % canopy density on Figure 5). However, the orientation of the channel influenced net solar radiation gains substantially under scenarios of 30-60 % canopy density (termed intermediate scenarios herein) (Figure 4a). We compare two channel orientations under a 30% canopy density in order to demonstrate the drivers of this variability (Figure 6). In the first scenario the channel was orientated SE-NW and the position of the vegetation did not provide shade from net solar radiation, as demonstrated by minimal overlap between the sun-path and the vegetation on Figure 6a. Consequently, the magnitude and diurnal pattern of modelled

net solar radiation (Figure 6b) was similar to those under sparse canopies (e.g. scenarios of 10 and 20 % density on Figure 5). In the second scenario the channel was orientated NW-SE and vegetation was located so that it shaded the channel when the sun was between south-easterly and south-westerly sky-positions, as demonstrated by the apex of the sun-path overlapping vegetation on Figure 6d. Consequently, the channel was shaded when potential net solar radiation gains were greatest (i.e. around mid-day) and so simulated values were low (Figure 6e). To summarise, large portions of the sky remained unhanded under intermediate scenarios (Figures 2c-2f). For all intermediate vegetation scenarios, large portions of the sky remained unshaded (Figures 2c-f) so that large net solar radiation gains were simulated when vegetation did not provide shade from the strongest gains whereas low net solar radiation gains when vegetation provided shade during these times (scenarios of 30-60% density on Figure 5).

4.1.2. Net energy

For each vegetation scenario and channel orientation, simulated daily total net energy flux is demonstrated in Figure 4b while the underlying diurnal patterns are demonstrated in Figure 7. Net energy flux was calculated in part as the sum of net longwave radiation, latent and sensible heat fluxes, which are dependent on water temperature. At each time step water temperature was not uniform throughout the reach, therefore modelled net energy at the upstream reach boundary is described in order to compare broad differences in energy loss from and gain to the water column between vegetation scenarios. Net energy exchange typically decreased as canopy density increased (Figure 4b). Beneath the sparsest canopies, the water column gained energy during daylight hours and lost energy overnight regardless of channel

orientation (scenarios of 10 and 20 % on Figure 7); this resulted in high daily total net energy gains to the water column under all channel orientations (Figure 4b). Channel orientation also had limited impact on net energy fluxes beneath the densest canopies where energy losses typically occurred during the day and overnight (scenarios of 70-90 % density on Figure 7), generating daily total net energy losses from the water column (Figure 4b). However, daily total net energy exchange was highly variable under intermediate vegetation scenarios of 30- 60 % canopy density (Figure 4b); the magnitude of energy gains or losses depended on channel orientation. We demonstrate the causes of this variability using the SE-NW (exposed to the greatest solar radiation gains) and NW-SE (shaded from the greatest solar radiation gains)) orientated channels under a 30% canopy density. The diurnal pattern and magnitude of net energy flux to the SE-NW orientated channel (Figure 6c) was similar to those under sparse canopies (e.g. scenarios of 10 and 20 % density on Figure 7) because vegetation did not shade the channel from the sun around mid-day (Figure 5a). In contrast, the NW-SE orientated channel was shaded from the sun by vegetation when net solar radiation inputs were greatest (Figures 6d and e) and small net energy losses or gains were simulated at these times (Figure 6f). For all intermediate vegetation scenarios (Figures 2d-g), large net energy gains were simulated when vegetation did not provide shade from the strongest net radiation gains; small net energy gains or losses were simulated when channels were shaded during these times (scenarios of 30- 60% canopy density on Figure 7).

4.2. Water temperature

4.2.1 Base water temperature model evaluation

The performance of the base water temperature model was evaluated previously by *Garner* et al. [2014] for a limited number of time steps between 1st and 7th July 2013 and deemed to be good. We calculated model evaluation statistics for the temperature of all water parcels released from AWS_{Open} on 6th July 2013 (i.e. statistics calculated from 23 time steps at 50 m intervals throughout the reach, thus n= 483 modelled values). Nash-Sutcliffe efficiency (0.97), percent-bias (-1.1 %), and mean error (-0.2 °C) were well-within limits proposed for watershed simulations of flow and constituent processes by *Moriasi* et al. [2007]. Furthermore, error (simulated minus observed values) in daily maximum (-0.6 °C), mean (-0.2 °C) and minimum (0.3 °C) water temperatures simulated throughout the reach demonstrated that temperatures were reproduced with high levels of accuracy.

4.2.2. Vegetation density and channel orientation effects on simulated water temperature dynamics

Water temperature metrics were derived from all values simulated throughout the reach (i.e. n= 483 temperatures). Typically, mean and maximum water temperatures decreased as vegetation density increased but minimum temperatures were not affected (Figure 8). Channel orientation had little effect on simulated water temperature dynamics under the sparsest (i.e. ≤ 20 %) and densest (i.e. ≥ 70 %) vegetation scenarios, as indicated in Figure 8 by little spread in the distribution of temperatures for these scenarios. Furthermore, under the densest canopies maximum temperatures simulated throughout the reach did not exceed the maximum inflow temperature at the upstream reach boundary (23.1 °C). Under canopies of intermediate density (i.e. 30- 60 %), varying channel orientation was associated with large variability in maximum and mean temperatures simulated throughout the reach

(Figure 8). For example under the 30 % canopy density scenario and low flow velocity, the highest maximum (27.9 °C) and mean (18.8 °C) temperatures were simulated for the SE-NW (exposed to the strongest solar radiation gains) orientated channel while the lowest maximum (23.6 °C) and mean temperatures (16.1 °C) were simulated for the NW-SE (shaded from the strongest solar radiation gains) orientated channel.

Spatio-temporal variability in temperature was also varied for intermediate canopy density scenarios. As an example we compare the SE-NW (exposed to the strongest solar radiation gains) and NW-SE (shaded from the strongest solar radiation gains) channel orientations under a 30 % canopy density. In comparison with the SE-NW orientated channel, the NW-SE orientated channel reduced water temperatures throughout the reach between around 11:00 and 17:00. The magnitude of the reduction increased in the downstream direction and greater reductions were observed under the low velocity condition (Figure 9c and f). For example at noon (when the effect was particularly prominent) under the high velocity condition and NW-SE orientation water temperatures were reduced by 0.3 °C at 50 m and 6.5 °C at 1050 m (Figure 9c). Under the low velocity condition and NW-SE orientation water temperatures were reduced by 2.8 °C at 50 m and 7.5 °C at 1050 m (Figure 9f). Furthermore, maximum temperatures occurred later in the day under the NW-SE orientation, around 18:00 versus around 12:00 under the SE-NW orientation.

4.2.3. Effects of water velocity on simulated water temperature dynamics

The velocity under which simulations were performed determined the residence time of water parcels within the reach. The high velocity scenario resulted in shorter

residence time (cf. low). For example the parcel of water released from AWS_{Open} under the high velocity scenario at 23:00 on 23 July left the reach around 00:45 on 24 July (Figure 9a and b) whereas under the low velocity scenario the water parcel did not leave the reach until around 11:30 on 24 July (Figure 9d and e).

Shorter (longer) residence times resulted in less (greater) heating and cooling of water. Consequently, simulations under the low velocity resulted in greater differences in temperatures between vegetation scenarios. Increasing vegetation density from 10- 90 % decreased mean temperatures by up to 5.4 °C (SE-NW orientation) for the low velocity scenario and 1.6 °C (NE-SW, E-W, SE-NW, S-N orientations) for the high velocity scenario (Figures 8a and d). Maximum temperatures decreased by 4.9 °C (all orientations) for the low velocity scenario and up to 3.0 °C (NE-SW, E-W, SW-NE, W-E, NW-SE orientations) for the high velocity scenario (Figures 8b and e). While minimum temperatures were reduced by up to 0.3 °C (E-W, SE-NW orientations) for the low velocity scenario and up to 0.5 °C (NE-SW, E-W, SE-NW, W-E orientations) for the high velocity scenario (Figures 8c and f). Furthermore, for each intermediate vegetation scenario (i.e. 30- 60 % density) the lower velocity enhanced differences in simulated temperatures between channel orientation scenarios. For example, under the high flow scenario and 30 % vegetation density temperatures varied by up to 0.8 °C for mean and 2.7 °C for maximum. Under the same vegetation scenario with a low velocity temperatures varied by 2.7 °C for mean and 4.3 °C for maximum (Figure 8). The effect of changing velocity was not confined to metrics; temperatures were modified throughout the reach at most time steps. Spatio-temporal differences between high and low velocity conditions are demonstrated in Figures 9g and 9h for a scenario of 30 % canopy density in which the

channel was orientated SE-NW (i.e. exposed to the strongest solar radiation gains) and a scenario of 30 % canopy density in which the channel was orientated NW-SE (i.e. shaded from the strongest solar radiation gains) respectively. Most notably, when the channel was exposed under the low velocity condition the highest temperatures (> 25.0 °C) occurred throughout most of the reach and persisted for longer (Figure 9g). When the channel was shaded under the low velocity condition the lowest daytime temperatures (< 20 °C) occurred throughout the reach and persisted for longer (Figure 9h).

5. DISCUSSION

This study quantified the influence of riparian vegetation density on energy exchange and water temperature dynamics in channels of varying orientation and with varying water velocity. The latter is a control of hydraulic retention time within the reach, which increases for lower gradient streams if wetted width and discharge are unchanged. The following discussion considers the effects of: (1) interactions between vegetation density and channel orientation on stream heating and cooling processes and (2) water velocity, and we identify the limitations of our approach. The implications of the findings are discussed in the context of river management in a changing climate.

5.1. Vegetation density, channel orientation and effects on stream heating and cooling

Riparian vegetation reduces solar radiation inputs and consequently net energy available to heat the water column [*Hannah* et al., 2004, 2008; *Leach and Moore*, 2010; *Garne*r et al., 2014, 2015]. During the study period (Northern Hemisphere

summer) at this relatively high latitude site (57°02'N) riparian vegetation had the greatest effect on net solar radiation and net energy inputs when it overhung the stream centreline and therefore shaded the stream from the greatest solar radiation inputs. Consequently during summer, when river flows are lowest and water temperature highest, riparian planting is only likely to be effective in reaches where river width is sufficiently narrow and/ or trees are sufficiently tall.

Around half of riparian vegetation scenarios did not typically reduce solar radiation sufficiently to produce net energy losses and therefore drive cooling of water as it travelled downstream. Previous research has demonstrated that under circumstances of net energy gain beneath a forested canopy, downstream reductions in instantaneous temperatures are generated when cool water that flows through exposed reaches overnight and during the early morning is advected through a forested reach and warms slowly due to greatly reduced net energy gains (*cf.* open reaches in which energy gains and thus rates of heating are greater) [see *Garner* et al., 2014]. The present study supports these observations; considerably lower maximum and mean temperatures were simulated when riparian canopies reduced net energy gains to the water column. However, net energy losses were simulated under the densest canopies (i.e. 70– 90 %) and some channel orientations under scenarios of intermediate (i.e. 40-60 %) canopy density so that maximum water temperatures within the reach did not exceed those at the upstream boundary. This suggests that under (1) very dense riparian canopies and (2) sparser canopies that provide shade when solar radiation inputs are greatest this energy flux may be blocked to such an extent that net energy losses occur and so water cools as it travels downstream. Scenarios of water cooling as it travelled downstream were not observed in an earlier study of the current riparian

vegetation condition in the reach [*Garner* et al., 2014] and so we recommend field investigation of these processes.

Previous studies have demonstrated that summary daily water temperature metrics (especially maxima) are reduced under the densest riparian canopies [*Broadmeadow* et al., 2011; *Groom* et al., 2011; *Imholt* et al., 2013] and that the orientation of vegetation relative to the path of the sun is important in determining the magnitude of this reduction [*Lee* et al., 2012]. Our study demonstrated that for intermediate canopy densities, the effect of riparian vegetation on maximum and mean temperatures is strongly dependent on channel orientation and thus the location of vegetation relative to the path of the sun. A canopy of 30 % density could be as effective at reducing maximum and mean temperatures as a canopy of 60 % density, provided that it shaded the water column when potential solar radiation gains were greatest (i.e. when the sun was between south-easterly and south-westerly sky positions in the Northern Hemisphere), while a canopy cover of up to 60 % could have little effect in reducing maximum and mean temperatures if it did not shade the channel while the sun was in these sky-positions.

River managers are increasingly searching for ways to reduce deleterious maximum temperatures. Re-introduction of riparian shading offers one of the most promising management approaches. Nevertheless, river managers must work within a broader social and economic context, where riparian planting (and associated fencing) comes with significant financial costs and has the potential to conflict with other landuses, which in the uplands of Scotland includes deer stalking and grouse shooting. Our study suggests that the channel must be shaded almost entirely to generate the greatest

reductions in mean and maximum temperatures, so this is an 'expensive' and potentially unachievable way to create thermal refugia. Such dramatic reductions may be desirable at locations where water temperatures are near, or anticipated to exceed, lethal or sub-lethal thresholds for an organism of interest [*Beechie* et al., 2013]. However extensive, dense shading can also have environmentally deleterious effects, such as: (1) reducing light levels, consequently primary production, macroinvertebrate consumers, and thus food availability for fish [*O'Grady*, 1993; *Kiffney* et al., 2004] and (2) increased surface roughness, filtration of airborne sulphur and nitrogen compounds and thus acidified waters [*Fowler* et al., 1989; *Malcolm* et al., 2014]. Consequently, the introduction of minimal shade targeted to appropriate headwater reaches may be the most cost-effective and ecologically beneficial method to generate cool-water refugia. Based on our results for Northern Hemisphere streams, optimal planting would take place on the most southerly bank of channels flowing east-west, northeast-southwest, or northwest-southeast, and *vice versa*. These planting locations could achieve considerable reductions in mean and maximum temperatures at minimal cost while minimising potential negative ecological consequences associated with dense shading. Channels that are orientated north-south, and *vice versa*, and thus do not have abundant southerly banks would require denser vegetation on their west and east banks to shade the water column from the highest solar radiation gains and thus yield reductions in water temperature. As such, they are likely to be a lower priority for targeted riparian planting schemes when reductions in stream temperature are a stated objective.

5.2. Effects of water velocity on stream heating and cooling

Mean and maximum water temperatures were increased and (to a lesser extent) minimum temperatures were decreased when water travelled at a low velocity (*cf.* high velocity) due to a longer residence time within the reach and thus greater accumulation/ dissipation of heat [*Subehi* et al., 2009; *Danehy* et al., 2005; *Groom* et al., 2011]. Consequently, our results suggest that riparian planting should be targeted in slow-flowing reaches, where retention times are longer and heat accumulation, and thus water temperatures, can be minimised most efficiently.

5.3 Limitations

Models are always simplifications of reality; therefore they must incorporate assumptions [*Westhoff* et al., 2011]. *Garner* et al. [2014] discuss in full the assumptions and consequent limitations of the base model. Here we identify the assumptions made in conducting the simulation experiments and make suggestions for improvements in future model applications.

In the experiments presented herein we sought to represent spatial variability in micro-climate through linear interpolation between relatively closely spaced AWS. The effects of spatially variable micro-climate have been often ignored in previous studies [e.g. *Rutherford* et al., 1997; *Watanabe* et al., 2005; *DeWalle*, 2008; *Lee* et al., 2012] but can modify turbulent fluxes and thus the energy budget significantly [e.g. *Hannah* et al., 2008; *Garner* et al., 2015]. We considered this approach to be reasonable for the base scenario and the good evaluation statistics suggest that this simple method was reasonable and appropriate.

Unfortunately, with only three AWS sites, it was not possible to separate the influence of riparian landuse from wider landscape effects on micro-climate. Consequently, we were unable to scale turbulent fluxes appropriately for the different landuse scenarios where this resulted in a spatial distribution of vegetation or channel orientation characteristics that differed from the base model. *Garner* et al. [2014] observed no clear relationship between the canopy densities and micrometeorological measurements at the three AWS locations used in this study hypothesising that micrometeorological measurements were therefore probably determined by a complex combination of landuse, riparian canopy density and interactions with surrounding topography, altitude and aspect. Consequently, changing the orientation of the channel and thus the location of vegetation (as in the simulation experiments) could modify micrometeorology in ways that would not be represented by our models where turbulent fluxes were effectively fixed from the base model. For example,vegetation located on a bank orientated into prevailing winds could provide more shelter and thus reduce wind speeds, latent heat and net energy exchange more than vegetation located on the opposite bank. Such processes were not represented here and we recognise that failure to counter balance changes in radiative fluxes with changes in evaporative fluxes under different vegetation scenarios could lead to biased model predictions of the effects of varying landuse and channel orientation on river temperature. Future work should therefore seek to generate an evidence base for improving the spatial representation of micrometeorological conditions beneath forest canopies of varying characteristics, thereby allowing for appropriate scaling of fluxes and incorporation into modelling studies such as this one.

Finally, we investigated the effects of changing velocity on water temperature but did not investigate the potential effects of spatially or temporally varying discharge and

did not consider the effects of changing velocity (for a fixed discharge) on wetted width. A full investigation of the effects of velocity, wetted width and discharge on river temperature could be conducted in future using channel geometry data in combination with hydraulic and hydrological models.

6. CONCLUSIONS

This study used field data from an upland Scottish salmon stream to underpin simulation experiments and provide systematic, mechanistic understanding of the effects of riparian shading scenarios, channel orientation and velocity on water temperature dynamics. The information gained from the novel modelling approach allows scientists and river managers to make better-informed decisions on optimal riparian tree planting strategies, through improved understanding of the inter-relationships between channel orientation and vegetation density that influence the effectiveness of riparian vegetation as a strategy for mitigating thermal extremes. The magnitude of reductions in water temperature under a given canopy density will depend on local conditions [*Ryan* et al., 2013] including the magnitude of net energy exchange (linked to meteorological conditions but also vegetation cover density and channel orientation), water velocity and hydrology. The experiments presented here demonstrate that where southerly banks (in the Northern Hemisphere) may be afforested then relatively sparse, overhanging vegetation is able to produce spatially and temporally extensive cool-water refugia when thermal extremes occur. Only in reaches where a southerly bank cannot be afforested is dense, overhanging vegetation required, and potentially deleterious effects should be considered in these circumstances. Additionally, planting should be targeted in slow-flowing (e.g. low

gradient) reaches where flow retention times are longer and within which large heat loads can accumulate in the absence of shade.

Scientists and river managers can use models such as those presented here to quantify potential changes in river thermal conditions associated with riparian planting schemes under both present and future climates at relatively small spatial scales. However these models require large observational datasets that are rarely available, and are logistically and financially unfeasible to collect in many circumstances. Consequently, future research should also seek to upscale the information yielded in this study to identify readily defined proxies for sensitivity (e.g. channel orientation and gradient) that can be combined with rapid riparian canopy density assessments [e.g. *Imholt* et al., 2013] in statistical models capable of predicting water temperatures at large spatial scales [e.g. *Hrachowitz* et al., 2010].

ACKNOWLEDGEMENTS

Grace Garner was funded by UK Natural Environment Research Council studentship NE/1528226/1. Anne Anckorn is thanked for cartographic assistance. Jason Leach and Dan Moore are thanked for generously sharing their net radiation model script. Marine Scotland Science Freshwater Laboratory staff provided field and technical assistance and maintained and downloaded weather stations. SEPA provided discharge data. We thank Xiaoming Cai for his assistance with Supplement 1. R was used for modelling and graphics. We are grateful to three anonymous reviewers for their constructive comments.

REFERENCES

Bartholow, J.M. (2000), The Stream Segment and Stream Network Temperature Models: A Self-Study Course. US Dept. of the Interior, US Geological Survey, Open-File Report 99-112

Beechie, T. H. Imaki, J. Greene, A. Wade, H. Wu, G. Pess, P. Roni, J. Kimball, J. Stanford, P. Kiffney P and N. Mantua (2013), Restoring salmon habitat for a changing climate, River Research and Applications, 29, 8, 939-960, doi: 10.1002/rra.2590

Beschta, R.L. (1997), Riparian shade and stream temperature: an alternative perspective, Rangelands, 19, 2, 25-28

Booth, D.B., and J.L. Leavitt (1999), Field evaluation of permeable pavement systems for improved stormwater management, Journal of the American Planning Association, 38, 3, 835-845, doi:10.1080/01944369908976060

Boyd, M. and B.V. Kasper (2003) Analytical methods for dynamic open channel heat and mass transfer: Methodology for heat source model Version 7.0, Oregon Department of Environmental Quality, Portland, OR, USA

Broadmeadow, S.B., J.G. Jones, T.E.L. Langford, P.J. Shaw, and T.R. Nisbet (2011), The influence of riparian shade on lowland stream water temperatures in southern England and their viability for brown trout, River Research and Applications, 27, 2, 226-237, doi: 10.1002/rra.1354

Brown, L.E., L. Cooper, J. Holden, and S.J. Ramchunder (2010), A comparison of stream water temperature regimes from open and afforested moorland, Yorkshire Dales, northern England, Hydrological Processes, 24, 22, 3206-3218, DOI: 10.1002/hyp.7746

Danehy, R.J., C.G. Colson, K.B. Parrett, and S.D. Duke (2005), Patterns and sources of thermal heterogeneity in small mountain streams within a forested setting. Forest Ecology and Management, 208, 1-3, 287–302, doi:10.1016/j.foreco.2004.12.006

DeWalle D.R. (2008) Guidelines for riparian vegetative shade restoration based upon a theoretical shaded-stream model, *Journal of the American Water Resources Association*, 44, 6, 1373-1387, doi: 10.1111/j.1752-1688.2008.00230.x

Evans, E.C., G.R. McGregor, and G.E. Petts (1998), River energy budgets with special reference to river bed processes, Hydrological Processes, 12, 4, 575–595, doi: 10.1002/(SICI)1099-1085(19980330)12:4<575::AID-HYP595>3.0.CO;2-Y

Frazer, G.W., C.D. Canham, and K.P. Lertzman (1999) Gap Light Analyzer (GLA), Version 2: Imaging Software to Extract Canopy Structure and Light Transmission Indices from True-Colour Fisheye Photographs, User's Manual and Program Documentation, Simon Frazer University and Institute of Ecosystem Studies, Millbrook, NY

Fowler, D., J.N. Cape, M.H., and Unsworth (1989), Deposition of atmospheric pollutants on forests, Philosophical Transactions of the Royal Society of London Series B- Biological Sciences, 324, 1223, 247-265, doi: http://dx.doi.org/10.1098/rstb.1989.0047

Garner, G, I.A. Malcolm, J.P. Sadler, and D.M. Hannah (2014), What causes cooling water temperature graidents in a forested stream reach?, Hydrology and Earth System Sciences, 18, 12, 5361-5376, doi:10.5194/hess-18-5361-2014

Garner, G., I.A. Malcolm, J.P. Sadler, C.P. Millar, and D.M. Hannah (2015), Inter-annual variability in the effects of riparian woodland on micro-climate, energy exchanges and water temperature of an upland Scottish stream, Hydrological Processes, 29, 6, 1080- 1095, doi: 10.1002/hp.10.223

Gomi, T., R.D. Moore, and A.S. Dhakal (2006), Headwater stream temperature response to clear-cut harvesting with different riparian treatments coastal British Columbia Canada, Water Resources Research 42, 8, W08437, doi: 10.1029/2005WR004162.

Groom, J.D., L. Dent, L.J. Madesn, and J. Fleuret (2011), Response of western Oregon (USA) stream temperature to contemporary forest management, Forest Ecology and Management, 262, 8, 1618-1629, doi:10.1016/j.foreco.2011.07.012

Hannah, D.M., I.A. Malcolm, C. Soulsby, and A.F. Youngson (2004), Heat exchanges and temperatures within a salmon spawning stream in the Cairngorms, Scotland: seasonal and sub-seasonal dynamics, River Research and Applications, 20, 6, 635–652, DOI: 10.1002/rra.771

Hannah, D.M., I.A. Malcolm, C. Soulsby, and A.F. Youngson (2008), A comparison of forest and moorland stream microclimate, heat exchanges and thermal dynamics, Hydrological Processes, 22,7, 919-940, doi: 10.1002/hyp.7003

Hannah, D.M., and G. Garner (2015), River water temperature in the United Kingdom: changes over the 20th century and possible changes over the 21st century, Progress in Physical Geography, 39, 1, 68-92, doi: 10.1177/0309133314550669

Hrachowitz, M., C. Soulsby, C. Imholt, I.A. Malcolm, and D. Tetzlaff (2010), Thermal regimes in a large upland salmon river: a simple model to identify the influence of landscape controls and climate change on maximum temperatures. Hydrological Processes, 24, 23, 3374-3391, doi: 10.1002/hyp.7756

Imholt, C., C.N. Gibbins, I.A. Malcolm, S. Langan, and C. Soulsby (2010), Influence of riparian tree cover on stream temperatures and the growth of the mayfly Baetis rhodani in an upland stream, Aquatic Ecology, 44, 4, 669-678, DOI: 10.1007/s10452-009-9305-0

Imholt, C., C. Soulsby, I.A. Malcolm, and C.N. Gibbins (2011), Influence of contrasting riparian forest cover on stream temperature dynamics in salmonid spawning and nursery streams, Ecohydrology, 6, 3, 380-392, doi: 10.1002/eco.1291

Imholt, C., C. Soulsby, I.A. Malcolm, M. Hrachowitz, C.N. Gibbins, S. Langan, and Tetzlaff D. (2013), Influence of scale on thermal characteristics in a large montane river basin, Ecohydrology, 29, 4,403-419, doi: 10.1002/rra.1608

Iqbal, M. (1983), An Introduction to Solar Radiation, Academic Press, Toronto

Johnson, S.L., and J.A. Jones (2000) Stream temperature responses to forest harvest and debris flows in Western Cascades Oregon, Canadian Journal of Fisheries and Aquatic Sciences, 57, 2, 30–39, doi: 10.1139/f00-109Jones (2000), Stream temperature responses to forest harvest and debris flows in western Cascades, Oregon, Canadian Journal of Fisheries and Aquatic Sciences, 57, 2, 30–39, doi: 10.1139/f00-109

Kiffney, P.M., J.S. Richardson, and J.P. Bull (2003), Responses of periphyton and insects to experimental manipulation of riparian buffer width along forest streams, Journal of Applied Ecology, 40, 6, 1060-1076, doi: 10.1111/j.1365-2664.2003.00855.x

Kurylyk, B.L., K.T.B. MacQuarrie, T. Linnansaari, R.A. Cunjak and R.A. Curry (2014), Preserving, augmenting, and creating thermal refugia in rivers concepts derived from research on the Miramichi River, New Brunswick (Canada), Ecohydrology, doi: 10.1002/eco.1566

Leach, J.A., and R.D. Moore (2010), Above stream microclimate and stream surface exchanges in a wildfire-disturbed riparian zone, Hydrological Processes, 24, 17, 2369-2381, doi: 10.1002/hyp.7639

Leach, J.A., and R.D. Moore (2011), Stream temperature dynamics in two hydrogeomorphically distinct reaches, Hydrological Processes, 25, 5, 679-690, doi: 10.1002/hyp.7854

Leach, J.A., R.D. Moore, S.G. Hinch, and T. Gomi (2012), Estimation of forest harvesting-induced stream temperature changes and bioenergetics consequences for cutthroat trout in a coastal stream in British Columbia, Canada, Aquatic Sciences, 74, 3, 427-441, doi: 10.1007/s00027-011-0238-z

Leach, J.A., and R.D. Moore (2014), Winter stream temperature in the rain-on-snow zone of the Pacific Northwest: influences of hillslope runoff and transient snow cover, Hydrology and Earth System Sciences, 18, 2, 819-838, doi:10.5194/hess-18-819-2014

LeBlanc, R.T., R.D. Brown and J.E. FitzGibbon (1997) Modelling the effects of land use change on water temperature in unregulated urban streams, Journal of Environmental Management, 49, 4, 445-469, doi: 10.1006/jema.1996.0106

Lee, T.Y., J.C. Huang, S.J. Kao, L.Y. Liao, C.S. Tzeng, C.H. Yang, P.K. Kalita, and C.P. Tung (2012), Modeling the effects of riparian planting strategies on stream temperature: Increasing suitable habitat for endangered Formosan Landlocked Salmon in Shei-Pa National Park, Taiwan, Hydrological Processes, 26, 24, 3635–3644, doi: 10.1002/hyp.8440

Li, G., C.R. Jackson and K.A. Kraseki (2012) Modeled riparian stream shading: Agreement with field measurements and sensitivity to riparian conditions, Journal of Hydrology, 428, 142-141, doi: 10.1016/j.jhydrol.2012.01.032

MacDonald, R.J., S. Boon, J.M. Byrne, and U. Sillins (2014a), A comparison of surface and subsurface controls on summer temperature in a headwater stream, Hydrological Processes, 28, 4, 2338-2347, doi: 10.1002/hyp.9756

MacDonald, R. J., S. Boon, J.M. Byrne and U. Silins (2014b) A process based stream temperature modelling approach for mountain regions, Journal of Hydrology, 511, 920–931, doi: 10.1016/j.jhdrol.2014.02.009

Malcolm, I.A., C. Souslby, A.F. Youngson, and D.M. Hannah (2005), Catchment scale controls on groundwater-surface water interactions: implications for the performance of juvenile salmonids. River Research and Applications, 21, 9, doi: 10.1002/rra.861

Malcolm, I.A., C.N. Gibbins, R.J. Fryer, J. Keay, D. Tetzlaff, and C. Soulsby (2014), The influence of forestry on acidification and recovery: insights from long-term hydrochemical and invertebrate data, Ecological Indicators, 37, B, 317-329, doi:10.1016/j.ecolind.2011.12.011

Moriasi, D.N., J.G. Arnold, M.W.N. Liew, R.D. Harmel, and T.L. Veith (2007), Model evaluation guidelines for systematic quantification of accuracy in watershed simulations, American Society of Agricultural and Biological Engineers, 50, 3, 885-900, doi: 10.13031/2013.23153

Moore, R.D., P. Sutherland, T. Gomi, and A. Dakal (2005), Thermal regime of a headwater stream within a clear-cut, coastal British Columbia, Hydrological Processes, 19, 13, 2591-2608, doi: 1 0.1002/hyp.5733

Moore, R.D., J.A. Leach, Knudson J.M. (2014) Geometric calculation of view factors for stream surface radiation modelling in the presence of riparian forest, Hydrological Processes, 28, 6, 2975-2986, doi: 10.1002/hyp.9848

O'Grady, M.F. (1993), Initial observations on the effects of varying levels of deciduous bankside vegetation on salmonid stocks in Irish waters, Aquatic Fisheries Management, 24, 4, 563-573, doi: 10.1111/j.1365-2109.1993.tb00631.x

Opperman, J.J., R. Luster, B.A. McKenney, M. Roberts, and A.W. Meadows (2010), Ecologically functional floodplains: connectivity, flow regime, and scale, Journal of the American Water Resources Association, 46, 2, 211-226, doi: 10.1111/j.1752-1688.2010.00426.x

Poole, G.C., and C.H. Berman (2001), An ecological perspective on in-stream temperature: Natural heat dynamics and mechanisms of human-caused degradation. Environmental Management, 27,6, 787-802, doi: 10.1007/s002670010188

Poole, G.C., S.J. O'Daniel, K.L. Jones, W.W. Woessner, E.S. Bernhardt, A.M. Helton, J.A. Stanford, B.R. Boer, and T. Beechie (2008), Hydrologic spiralling: the role of multiple interactive flow paths in stream ecosystems, River Research and Applications, 24, 7, 1018-1031, doi: 10.1002/rra.1099

Prata, A.J. (1996), A new long-wave formula for estimating downward clear-sky radiation at the surface, Quarterly Journal of the Royal Meteorological Society, 122, 553, 1127–1151, doi: 10.1002/qj.49712253306

R Core Team, R: A Language and Environment for Statistical Computing, R Foundation for Statistical Computing, Vienna, Austria, http://www.R-project.org, last access: 25 September 2013

Roth, T.R., M.C. Westhoff, H. Huwald, J.A. Huff, J.F. Rubin, G. Barrenetxea, M. Vettereli, A. Parriaux, J.S. Selker, and M.B. Parlange (2010), Stream temperature response to three riparian vegetation scenarios by use of a distributed temperature validated model, Environmental Science and Technology, 44, 6, 2072-2078, doi: 10.1021/es902654f

Rutherford J.C., S. Blackett, C. Blackett, L. Saito, R.J. Davies-Colley (1997) Predicting the effects of shade on water temperature in small streams, New Zealand

Journal of Marine and Freshwater Research, 31, 5, 707-721, doi: 10.1080/00288330.1997.9516801

Rutherford, J. C., N.A. Marsh, P.M. Davies and S.E. Bunn (2004) Effects of patchy shade on stream water temperature: how quickly do small streams heat and cool?, Marine and Freshwater Research, 55, 737– 748, 2004, doi: 10.1071/MF04120

Ryan, D.K., J.M. Yearsley, and M. Kelly-Quinn (2013), Quantifying the effect of semi-natural riparian cover on stream temperatures: implications for salmonid habitat management, Fisheries Management and Ecology, 20, 6, 494-507, doi: 10.1111/fme.12038

Soetaert, K., T. Petzoldt, and R. Woodrow Setzer (2010), Solving differential equations in R: package deSolve, Journal of Statistical Software, 33, 9, 1-25

Story, A., R.D. Moore, and J.S. Macdonald (2003), Stream temperatures in two shaded reaches below cutblocks and logging roads: downstream cooling linked to subsurface hydrology, Canadian Journal of Forest Research. 33, 8, 1383–1396, doi: 10.1139/x03-087

Subehi, L., T. Fukushima, Y. Onda, S. Mizugaki, T. Gomi, T. Terajima, K. Kosugi, S. Hiramatsu, H. Kitahara, K. Kuraji, and N. Ozaki (2009), Influences of forested watershed conditions on fluctuations in stream water temperature with special reference to watershed area and forest type, Limnology, 10, 1, 33-45, doi: 10.1007/s10201-008-0258-0

Stull, R.B. (2000) Meteorology for Scientists and Engineers. Brooks/ Cole, Pacific Grove

Tetzlaff, D., C. Soulsby, C. Gibbins, P.J. Bacon, and A.F. Youngson (2005), An approach to assessing hydrological influences on feeding opportunities of juvenile

Atlantic salmon (Salmo salar): a case study of two contrasting years in a small, nursery stream, Hydrobiologia, 549, 1, 65-77, doi: 10.1007/s10750-005-4166-6

Tetzlaff, D., C. Soulsby, S. Waldron, I.A. Malcolm, P.J. Bacon, S.M. Dunn, A. Lilly, and A.F. Youngson (2007), Conceptualisation of runoff processes using a geographical information system and tracers in a nested mesoscale catchment, Hydrological Processes, 21, 10, 1289-1307, doi: 10.1002/hyp.6309

Upper Dee riparian scheme, The River Dee Trust: http:// www.theriverdeetrust.org.uk/information/ourwork.asp (last access: 14 January 2016), 2011.

Van vliet, M.T.H., F. Ludwig, and P. Kabat (2013), Global streamflow and thermal habitats of freshwater fishes under climate change, Climatic Change, 121, 4, 739-754, doi: 10.1007/s10584-013-0976-0

Watanabe, M., R.M. Adams, J. Wu, J.P. Bolte, M.M. Cox, S.L. Johnson, W.J. Liss, W.G. Boggess, J.L., and Ebersole JL (2005), Toward efficient riparian restoration: integrating economic, physical and biological models, Environmental Management, 75, 2, 92-104, doi:10.1016/j.jenvman.2004.11.005

Webb, B.W., and Y. Zhang (1997), Spatial and seasonal variability in the components of the river heat budget, Hydrological Processes, 111, 79–101, doi: 10.1002/(SICI)1099-1085(199701)11:1<79::AID-HYP404>3.3.CO;2-E

Westhoff M.C., H.H.G. Savenije, W.M.J. Luxemburg, G.S. Stelling, N.C. van de Giesen, J.S. Selker, L. Pfister, and S. Uhlenbrook (2007), A distributed stream temperature model using high resolution temperature observations, Hydrology and Earth System Sciences, 11, 1469-1480, doi: 10.5194/hess-11-1469-2007

Westhoff, M.C., M.N. Gooseff, T.A. Bogaard, and H.H.G. Savenije (2011), Quantifying hyporheic exchange at high spatial resolution using natural temperature

variations along a first-order stream, Water Resources Research, 47, 10, W10508, doi: 10.1029/2010WR009767

Wilby, R.L., H.G. Orr, G. Watts, R.W. Battarbee, P.M. Berry, R. Chadd, S.J. Dugdale, M.J. Dunbar, J.A. Elliott, C. Extence, D.M. Hannah, N. Holmes, A.C. Johnson, B. Knights, N.J. Milner, S.J. Ormerod, D. Solomon, R. Timlett, P.J. Whitehead J, and P.J. Wood (2010), Evidence needed to manage freshwater ecosystems in a changing climate: turning adaptation principles into practice. Science of the Total Environment, 408, 19, 4150–4164, doi: 10.1016/j.scitotenv.2010.05.014

Figure captions

Figure 1. Girnock Burn (a) location within Scotland (b) catchment map (c) locations of field data collection sites

Figure 2. Hemispherical images used to represent (a) 10% (b) 20% (c) 30% (d) 40% (e) 50% (f) 60% (g) 70% (h) 80% (i) 90% riparian canopy density scenarios. Eight coloured lines in each image represent the path of the sun across the sky relative to changing north in each image at 45-degree increments

Figure 3. Model input data for 6 July 2013 (a) air and water temperatures (b) solar radiation (c) wind speed (d) relative humidity (e) discharge

Figure 4. Simulated daily total (a) net solar radiation (b) net energy flux at the upstream reach boundary under each vegetation scenario and channel orientation. Eight coloured points in each plot represent the path of the sun across the sky relative to changing north in each image at 45-degree increments

Figure 5. Simulated net solar radiation at the upstream reach boundary under each vegetation scenario and channel orientation. Eight coloured lines in each image represent the path of the sun across the sky relative to changing north in each plot at 45-degree increments. [solar radiation receipt varied indiscernibly with channel orientation under scenarios of 10 and 20% canopy density and are therefore illustrated by a single black line]

Figure 6. (a) Hemispherical image and sun-path (b) net solar radiation (c) net energy under 30 % canopy density and channel SE-NW orientation. (d) Hemispherical image and sun-path (e) net solar radiation (f) net energy under 30 % canopy density and NW-SE channel orientation.

Figure 7. Simulated net energy flux at the upstream reach boundary under each vegetation scenario and channel orientation. Eight coloured lines in each plot represent the path of the sun across the sky relative to changing north in each image at 45-degree increments. [net energy flux varied indiscernibly with channel orientation under scenarios of 10 and 20% canopy density and are therefore illustrated by a single black line]

Figure 8. Simulated mean (a,d), maximum (b,e) and minimum (c,f) water temperatures for (a-c) high flow velocity and (d-f) low flow velocity scenarios. Eight coloured points in each plot represent the path of the sun across the sky relative to changing north in each image at 45-degree increments

Figure 9. Water temperatures (z-axis, °C) simulated throughout the reach under the scenario of 30% canopy density (a) southerly sky-positions exposed and high flow velocity (b) southerly sky-positions shaded and high flow velocity (c) effect of shading [b minus a] under high velocity (d) southerly sky-positions exposed and low flow velocity (e) southerly sky positions shaded and low flow velocity (f) effect of shading [e minus d] under low velocity (g) effects of velocity under high exposure [d minus a] (h) effects of velocity under low exposure [f minus c]

a

N

Inverness

Field Site

Aberdeen

Dundee

b

Map c

400

300

400

500

400

500

500

500

N

0 1 km

Unmanaged semi-natural forest

C

AWS_{Open}

AWS_{FUS}

AWS_{FDS}

Water temperature logger

Littlemill gauging station

N

0 1 km

300

260

350

260

300

350

400

300

350

300

350

400

Figure

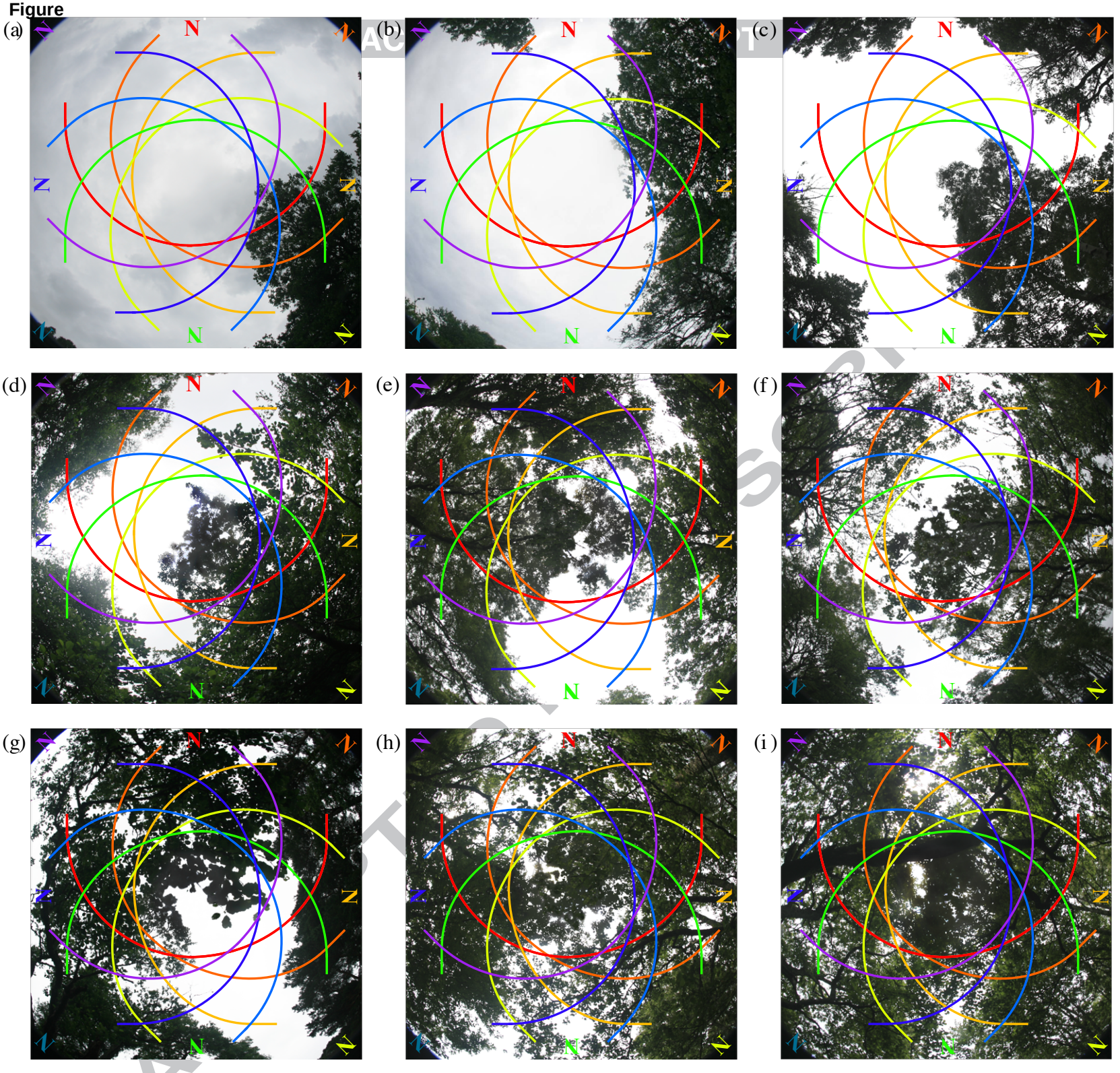
(a)
(b)
(c)
(d)
(e)
(f)
(g)
(h)
(i)
North-South
North East-South West
East- West
South East-North West
South- North
South West-North East
West- East
North West-South East

Figure

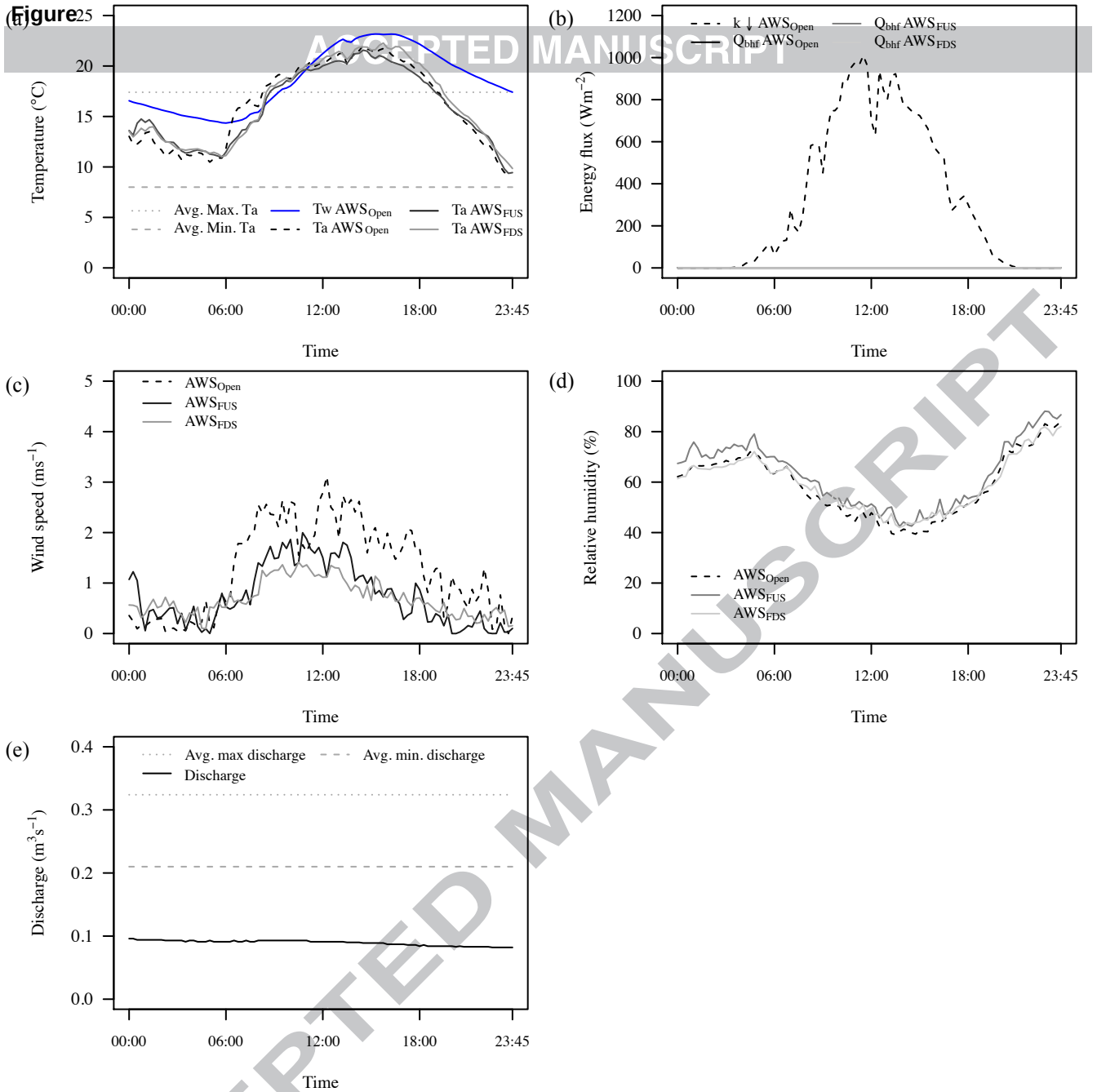

Figure

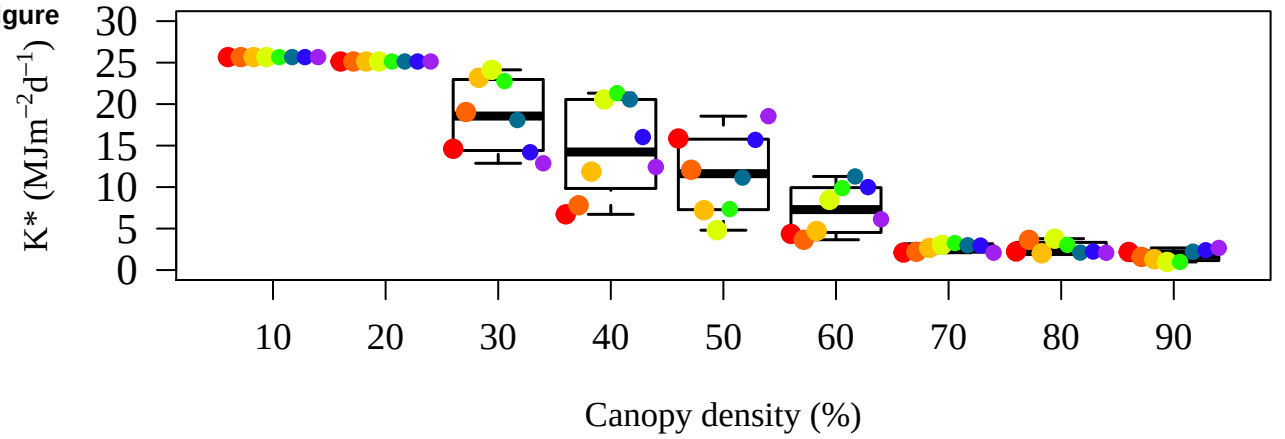
K* (MJm^{-2}d^{-1})
30
25
20
15
10
5
0
10
20
30
40
50
60
70
80
90
Canopy density (%)

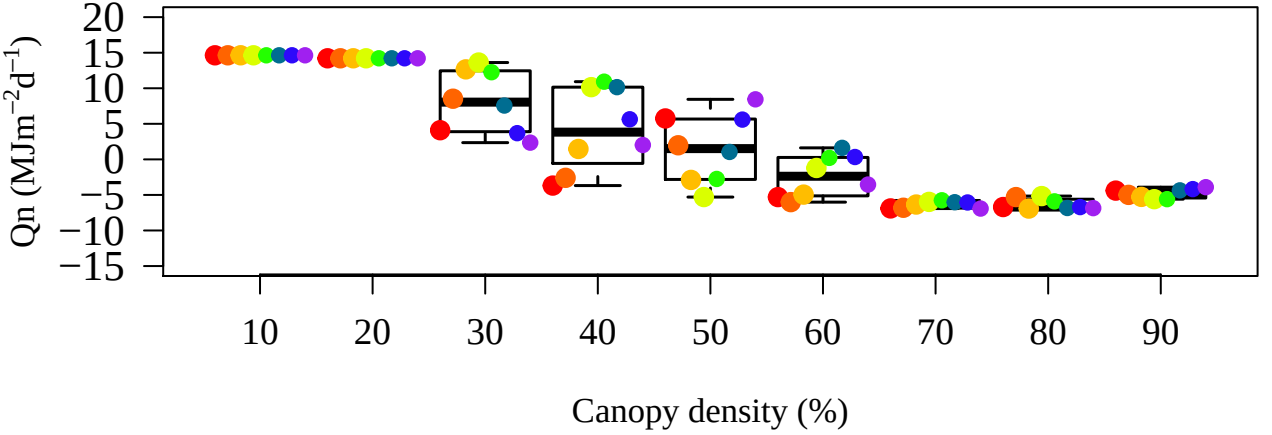
Qn (MJm^{-2}d^{-1})
20
15
10
5
0
−5
−10
−15
10
20
30
40
50
60
70
80
90
Canopy density (%)

Figure

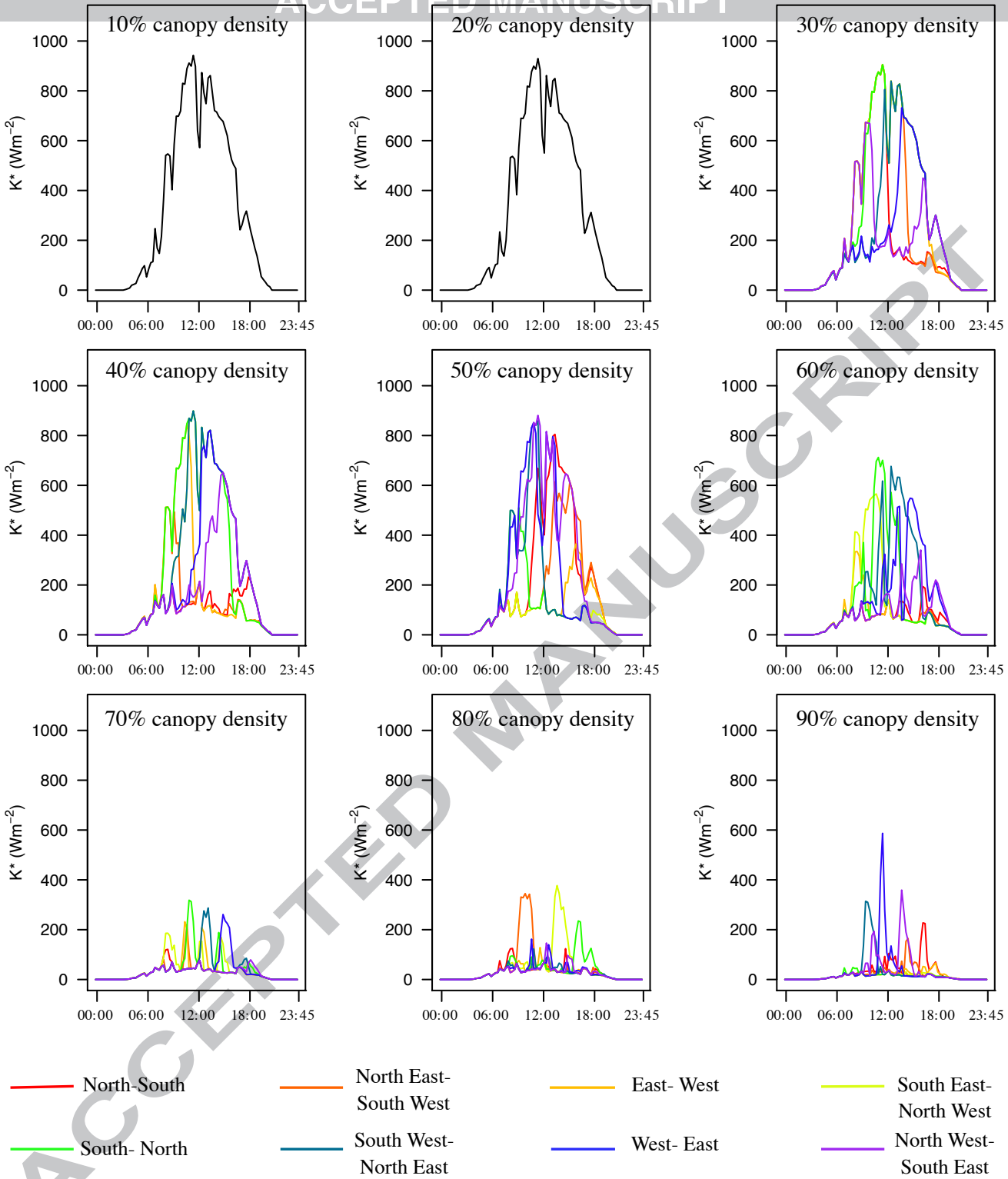

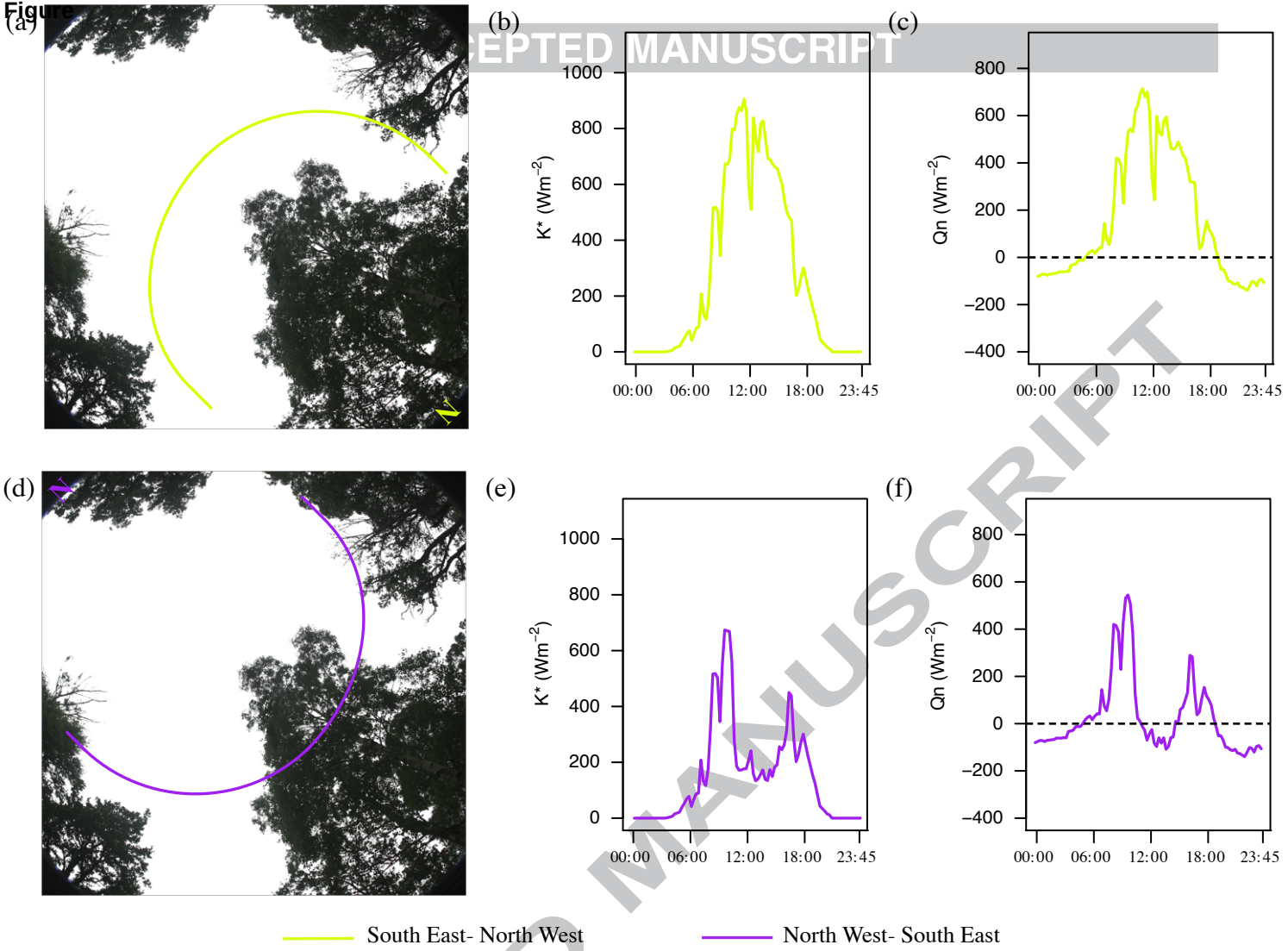

Figure

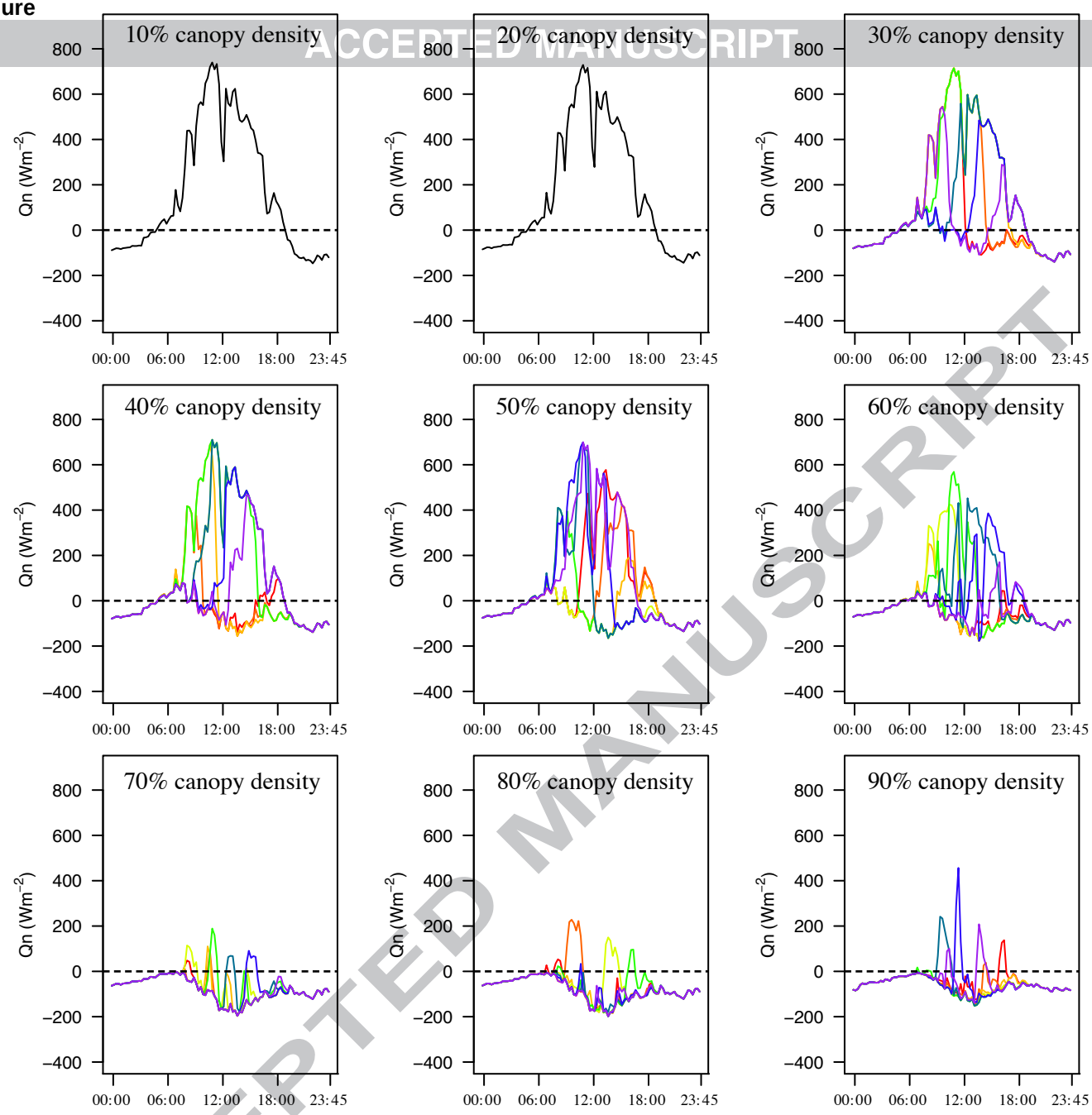

Figure

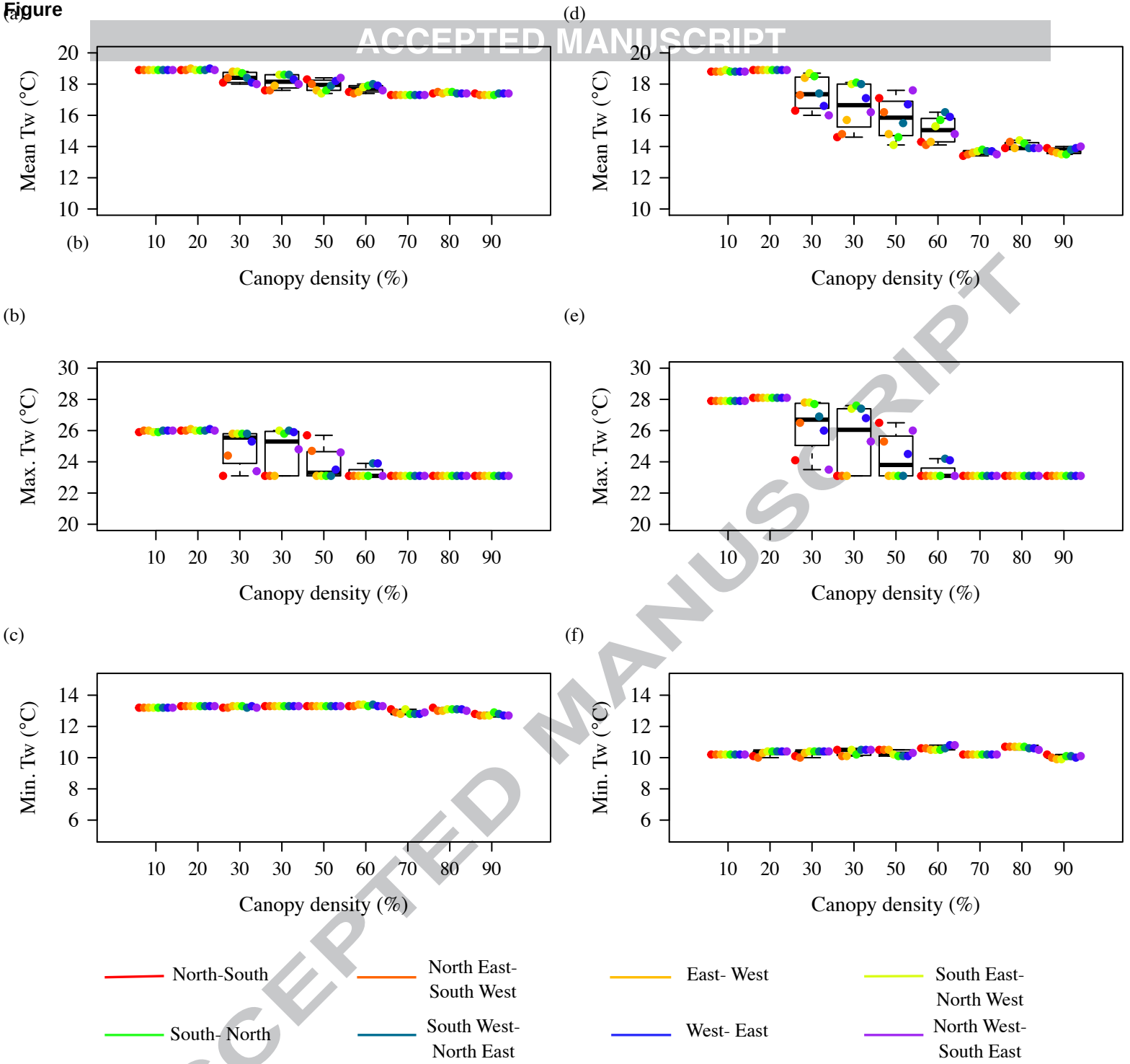

Figure

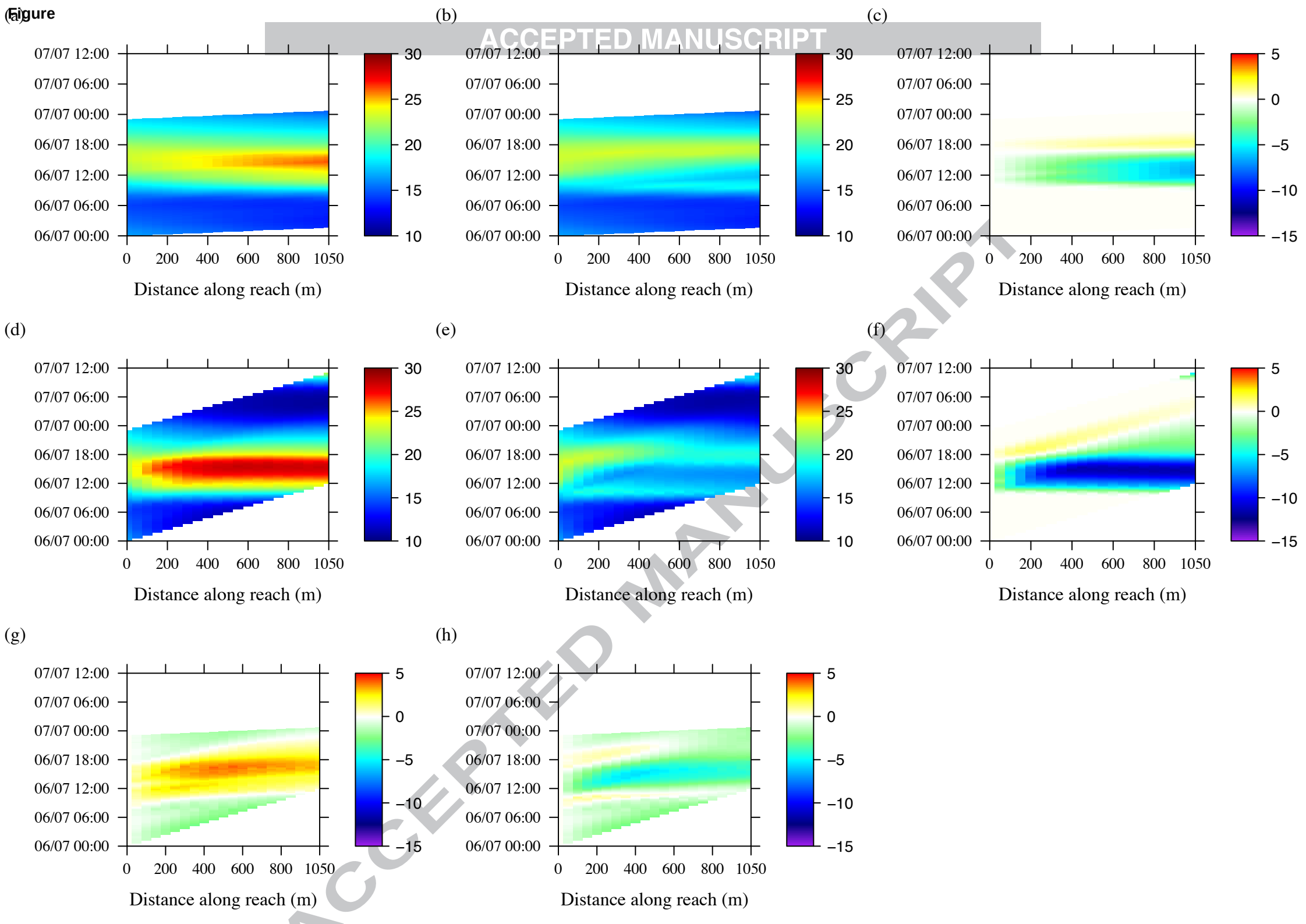

Highlights

1. Canopy density, river orientation and water velocity interact to influence water temperature
2. Channel orientation and water velocity should determine optimal planting strategies
3. Sparse riparian canopies can generate spatio- temporally extensive cool water refugia